Supporting Information

An Efficient and Robust Lanthanum Strontium Cobalt Ferrite Catalysts as a Bifunctional Oxygen Electrode for Reversible Solid Oxide Cells

Doyeub Kim[a, †], Jin Wan Park[c, †], Munseok S. Chae[c, †], Incheol Jeong[c], Jeong Hwa Park[c], Kyeong Joon Kim[a], Jong Jun Lee[c], Chanhoon Jung[c], Chan-Woo Lee[b, *], Seung-Tae Hong[c, *], and Kang Taek Lee[a, *]

[a]*Department of Mechanical Engineering, Korea Advanced Institute of Science and Technology (KAIST), Daejeon, 34141, Republic of Korea*

[b]*Platform Technology Laboratory, Korea Institute of Energy Research (KIER), Daejeon, 34129, Republic of Korea*

[c]*Department of Energy Science and Engineering, Daegu Gyeongbuk Institute of Science and Technology (DGIST), Daegu 42988, Republic of Korea*

[†] These authors contributed equally to this work

[*]Corresponding Authors: leekt@kaist.ac.kr, st.hong@dgist.ac.kr, and cwandtj@kier.re.kr

Contents:

Table S1-S5, Fig. S1-S15

Table S1. Comparison of selected interatomic distances (Å) in the structure of LSCF2882 and LSCF6428 at room temperature.

Type of atomic bonding	Interatomic distances (Å)	
	LSCF2882	LSCF6428
La1/Sr1-O1	2.724(1) Å × 12	2.490(6) Å × 3 2.754(1) Å × 6 3.017(6) Å × 3
Co1/Fe1-O1	1.926(1) Å × 6	1.960(1) Å × 6
O1-O1	2.724(1) Å	2.755(2) Å 2.791(1) Å

Table S2. Comparison of selected interatomic angles (°) in the structure of LSCF2882 and LSCF6428 at room temperature.

Type of atomic bonding	Interatomic angle (°)	
	LSCF2882	LSCF6428
O1- Co1/Fe1-O1	90.000(1)°	89.24(2)° 90.75(2)°
O1-La1/Sr1-O1	60.000(1)° 90.000(1)°	84.52(1)° 60.87(3)° 63.12(8)°

Table S3. k_{chem} and D_{chem} values for LSCF2882 and LSCF6428 as functions of temperature from 650 to 800 °C.

Temperature (°C)	LSCF2882		LSCF6428	
	k_{chem} (cm s^{-1})	D_{chem} (cm^2 s^{-1})	k_{chem} (cm s^{-1})	D_{chem} (cm^2 s^{-1})
800	3.24×10^{-3}	1.03×10^{-4}	1.39×10^{-3}	6.69×10^{-6}
750	1.81×10^{-3}	6.81×10^{-5}	6.74×10^{-4}	4.28×10^{-6}
700	1.12×10^{-3}	5.13×10^{-5}	4.57×10^{-4}	2.52×10^{-6}
650	7.66×10^{-4}	1.76×10^{-5}	1.62×10^{-4}	1.72×10^{-6}

Table S4. Calculated volume expansion of the cell for LSCF2882 and LSCF6428 by introducing oxygen vacancies.

	LSCF2882	LSCF6428
Pristine model ($Å^3$)	459	448
Vacancy model ($Å^3$)	466	459
Expansion (%)	1.53	2.41

Table S5. Elementary ORR processes and corresponding reaction orders.

Elementary Reactions		Reaction order (n)	Ref
Adsorption of oxygen	$O_{2(g)} \leftrightarrow O_{2,ad}$	1	1,2,4
Dissociation of adsorbed oxygen	$O_{2,ad} \longrightarrow 2O_{ad}$	1/2	3,4
Charge Transfer	$O_{ad} + e^{'} \longrightarrow O_{ad}^{'}$ $O_{TPB}^{'} + e^{'} \longrightarrow O_{TPB}^{''}$	1/4	1,4
Oxygen ion incorporation	$O_{TPB}^{''} + V_{O}^{\cdot\cdot} \leftrightarrow O_{O}^{X}$	1/10	1,3

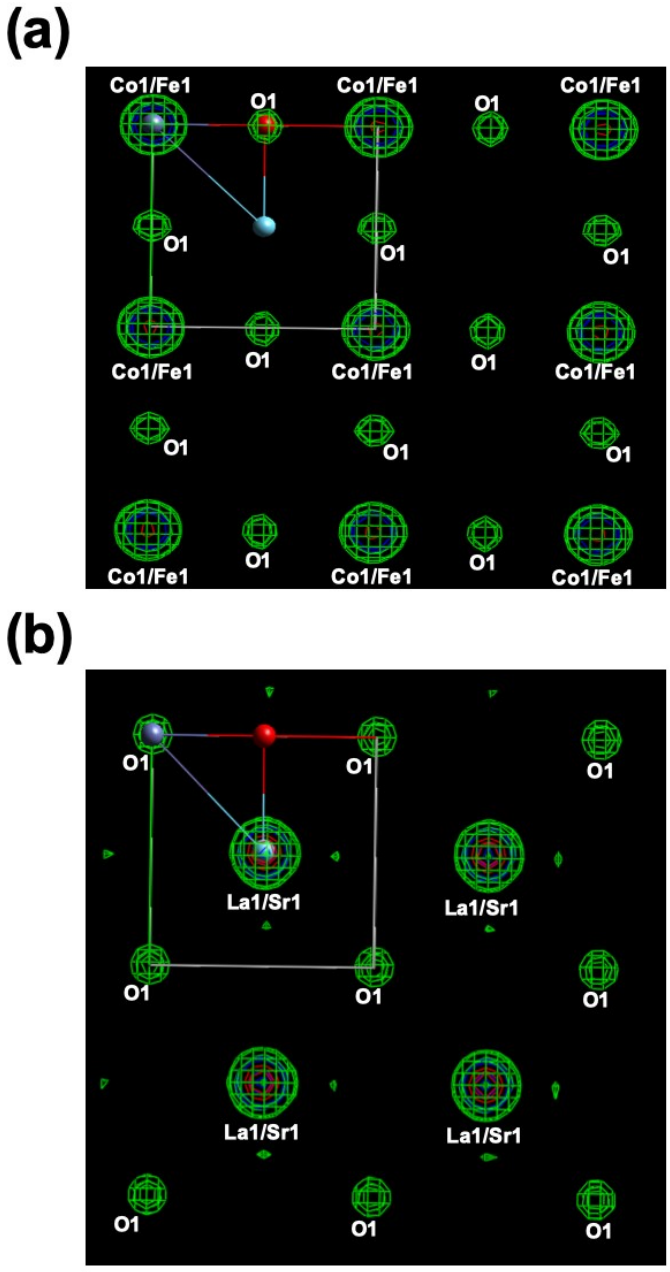

Figure S1. (001) view of the observed Fourier map for LSCF2882. The map width is 10.3 Å, and the center is at (a) (Co1/Fe1) and (b) (O1), respectively. All the densities are at the Co1/Fe1, and La1/Sr1 planes, respectively.

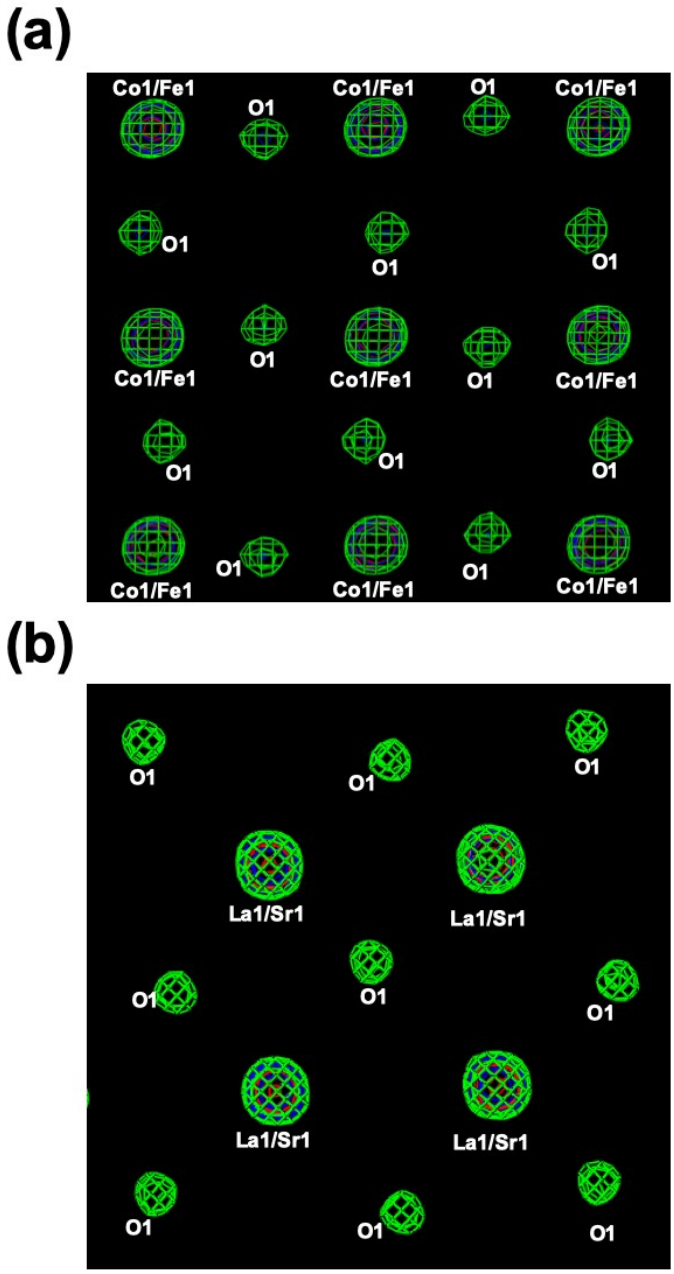

Figure S2. (201) view of the observed Fourier map for LSCF6428. The map width is 10.3 Å, and the center is at (a) (Co1/Fe1) and (b) (O1), respectively. All the densities are at the Co1/Fe1, and La1/Sr1 planes, respectively.

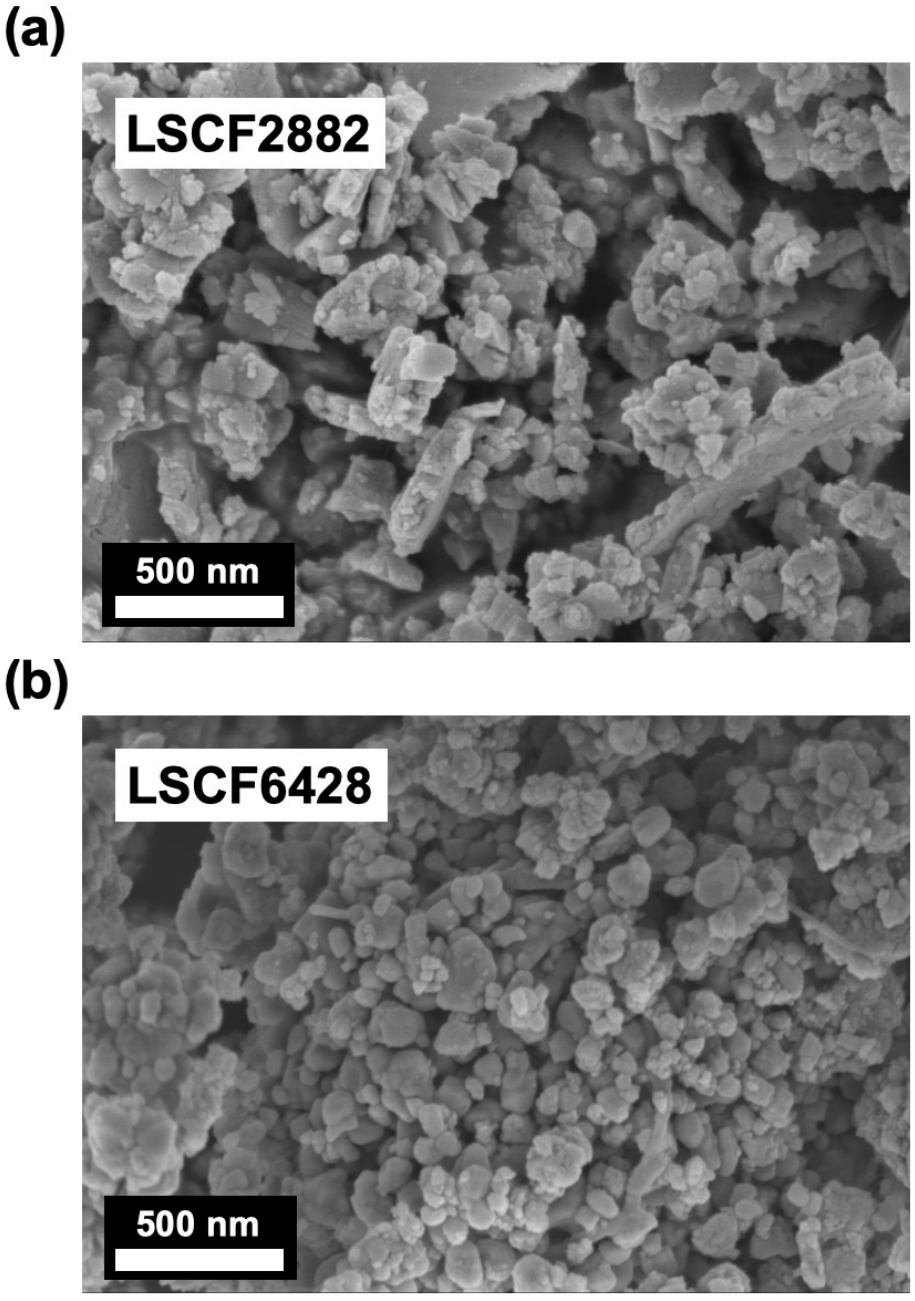

Figure S3. Microstructure analysis of (a) LSCF2882 and (b) LSCF6428 oxygen electrodes.

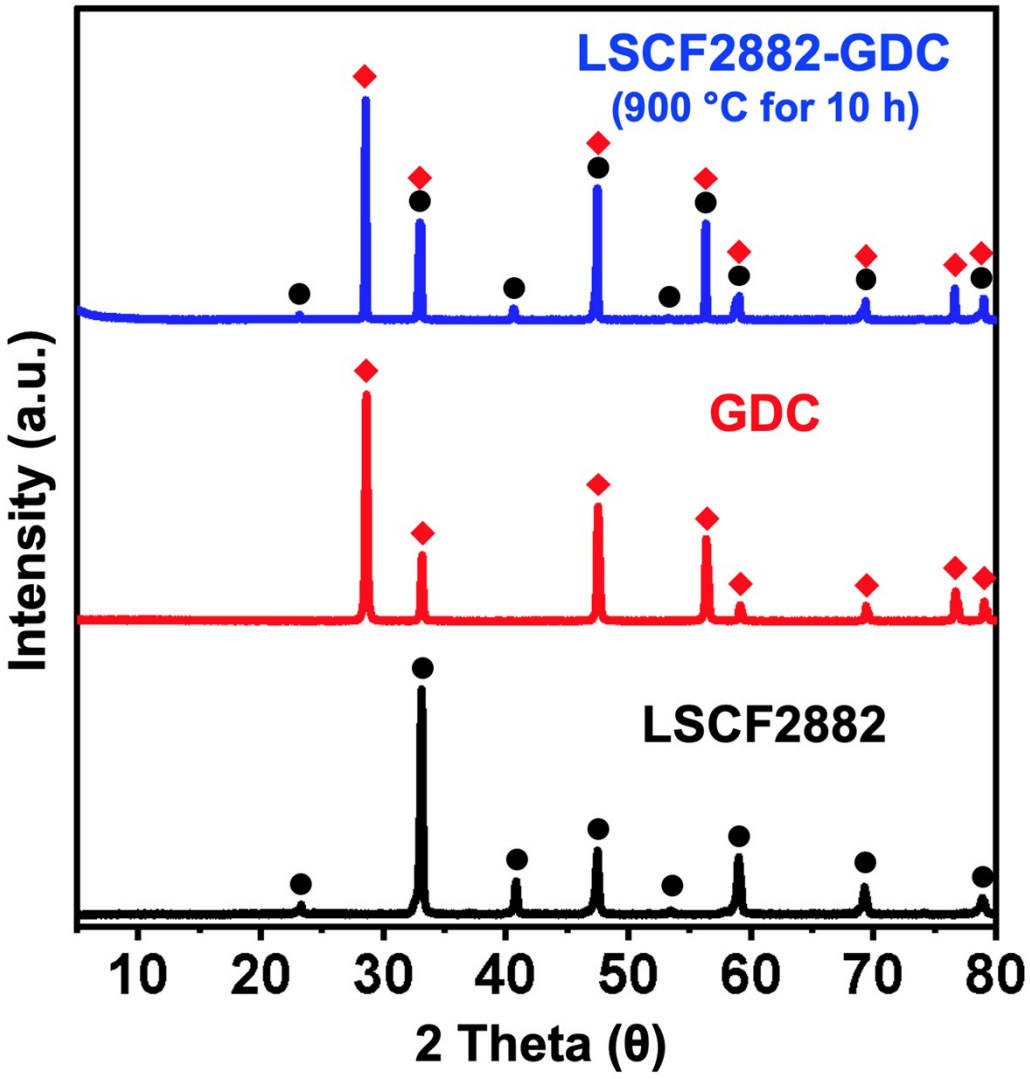

Figure S4. XRD results of the mixture of LSCF2882 and GDC powders annealed at 900 °C for 10 h in ambient air.

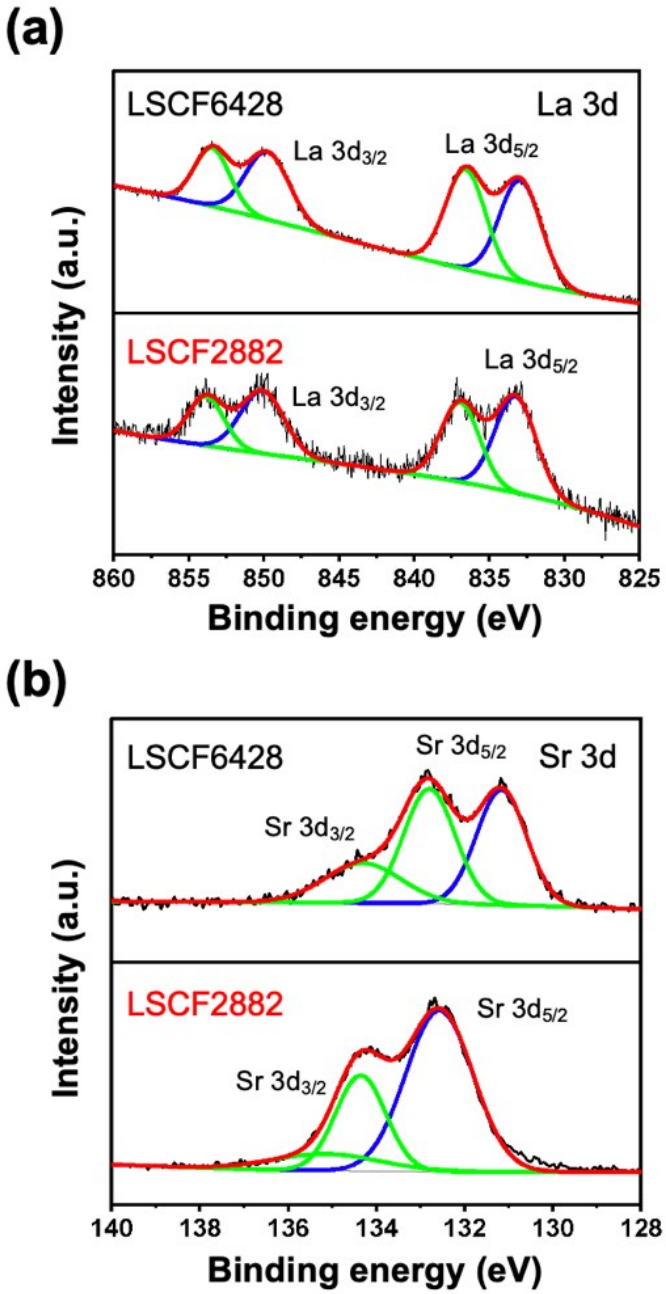

Figure S5. XPS spectra of (a) La 3d, and (b) Sr 3d for LSCF2882 and LSCF6428.

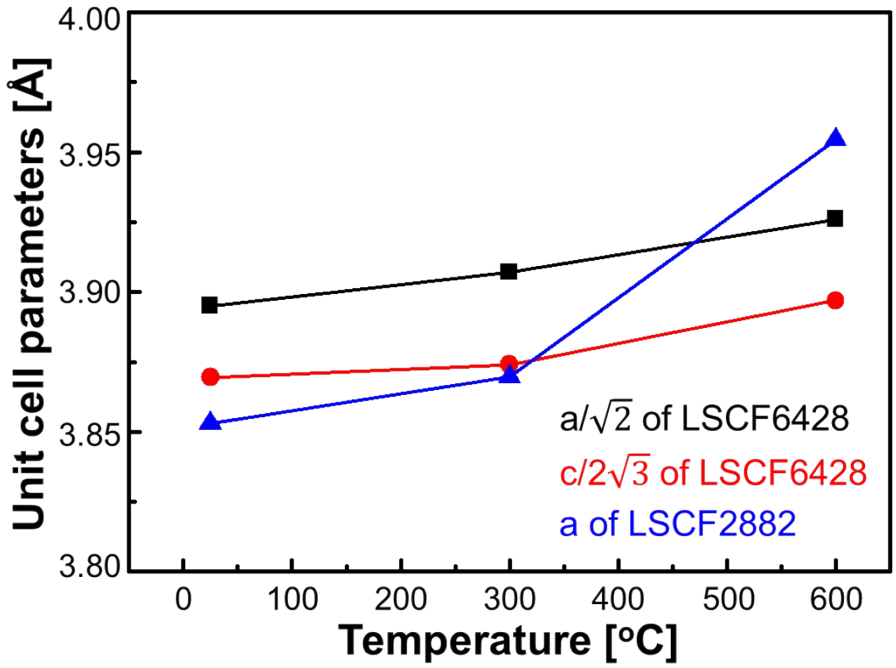

Figure S6. Evolution of unit cell parameters (*a*, *b* and *c*), and volume in LSCF2882 and LSCF6428 upon temperature increase.

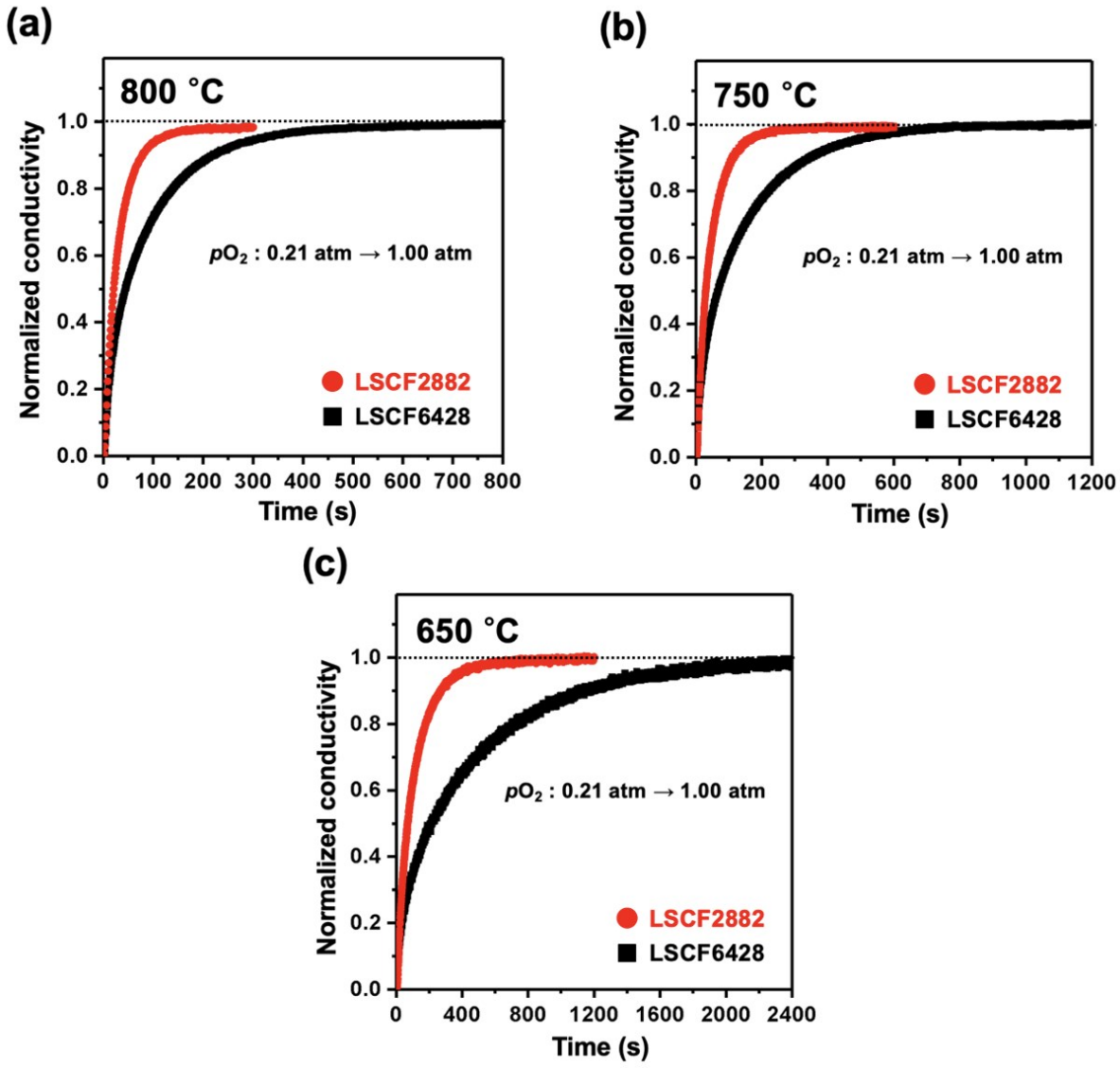

Figure S7. Comparison of resultant normalized conductivity relaxation curves for LSCF2882 and LSCF6428 at (a) 800, (b) 750, and (c) 650 °C.

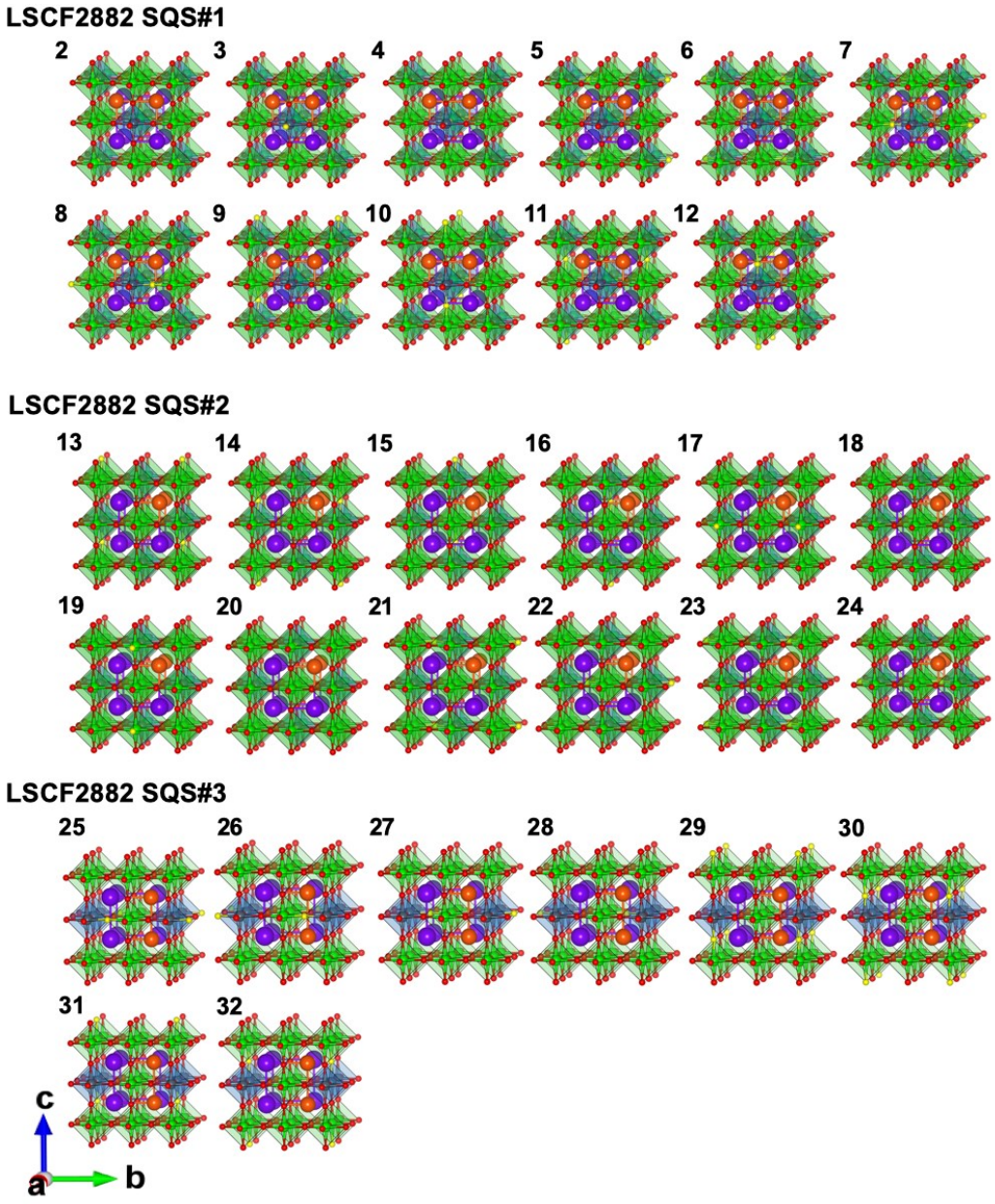

Figure S8. 31 single vacancy models from three SQS structures for LSCF2882 (first model is shown in Fig. 4a).

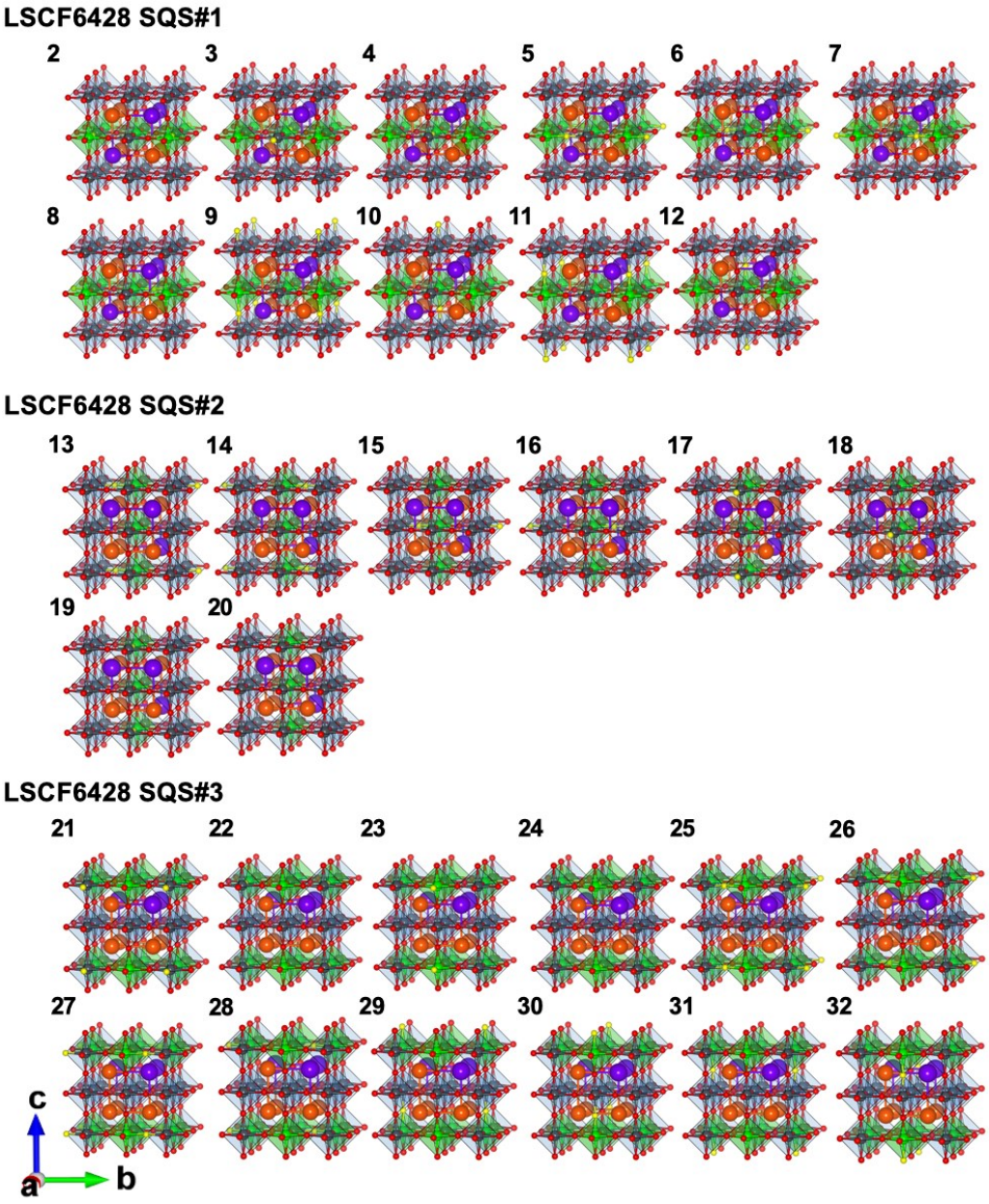

Figure S9. 31 single vacancy models from three SQS structures for LSCF6428 (first model is shown in Fig. 4b).

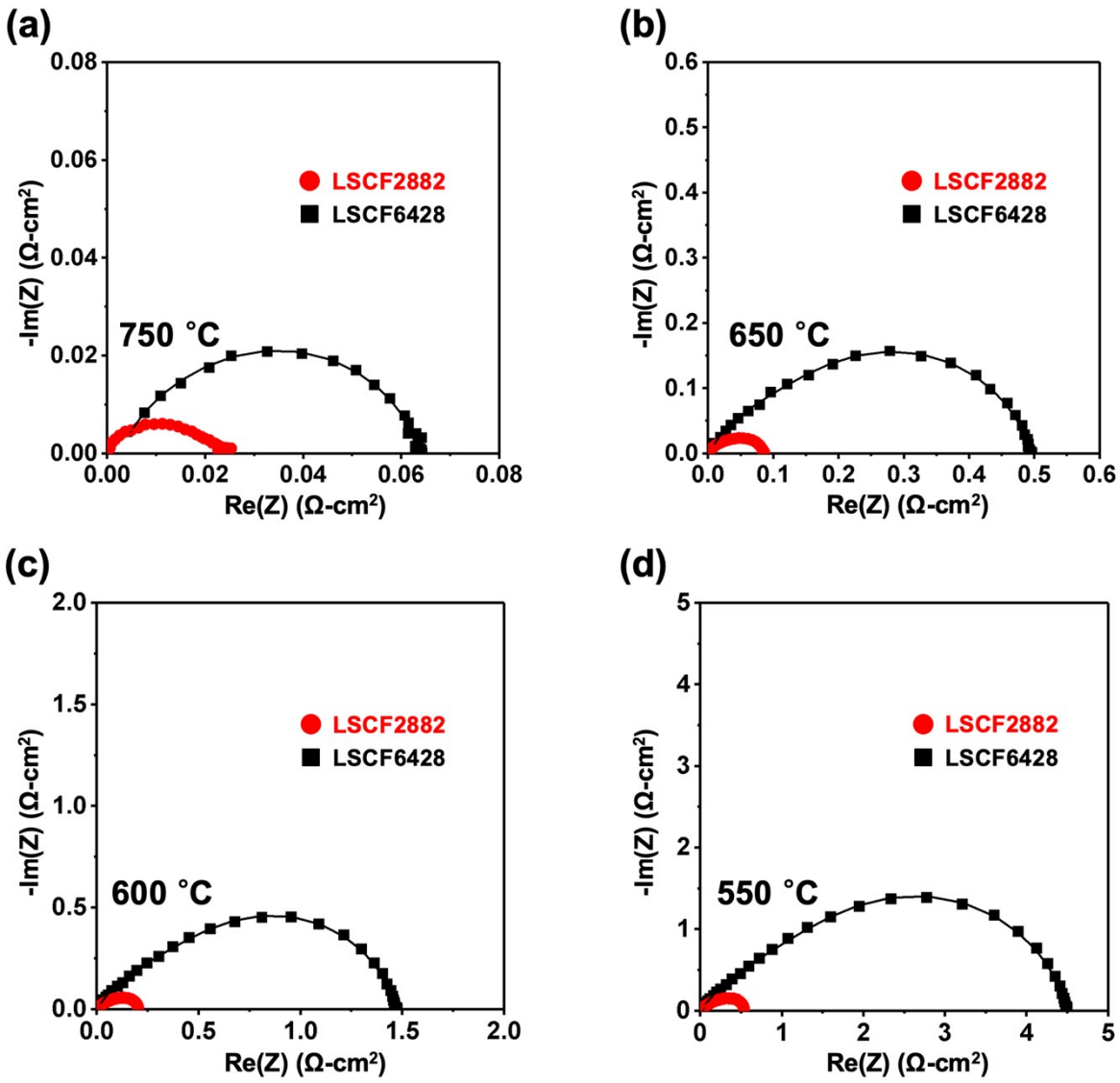

Figure S10. Nyquist plots of symmetrical cells at (a) 750, (b) 650, (c) 600, and (c) 550 °C for LSCF2882 and LSCF6428 oxygen electrodes.

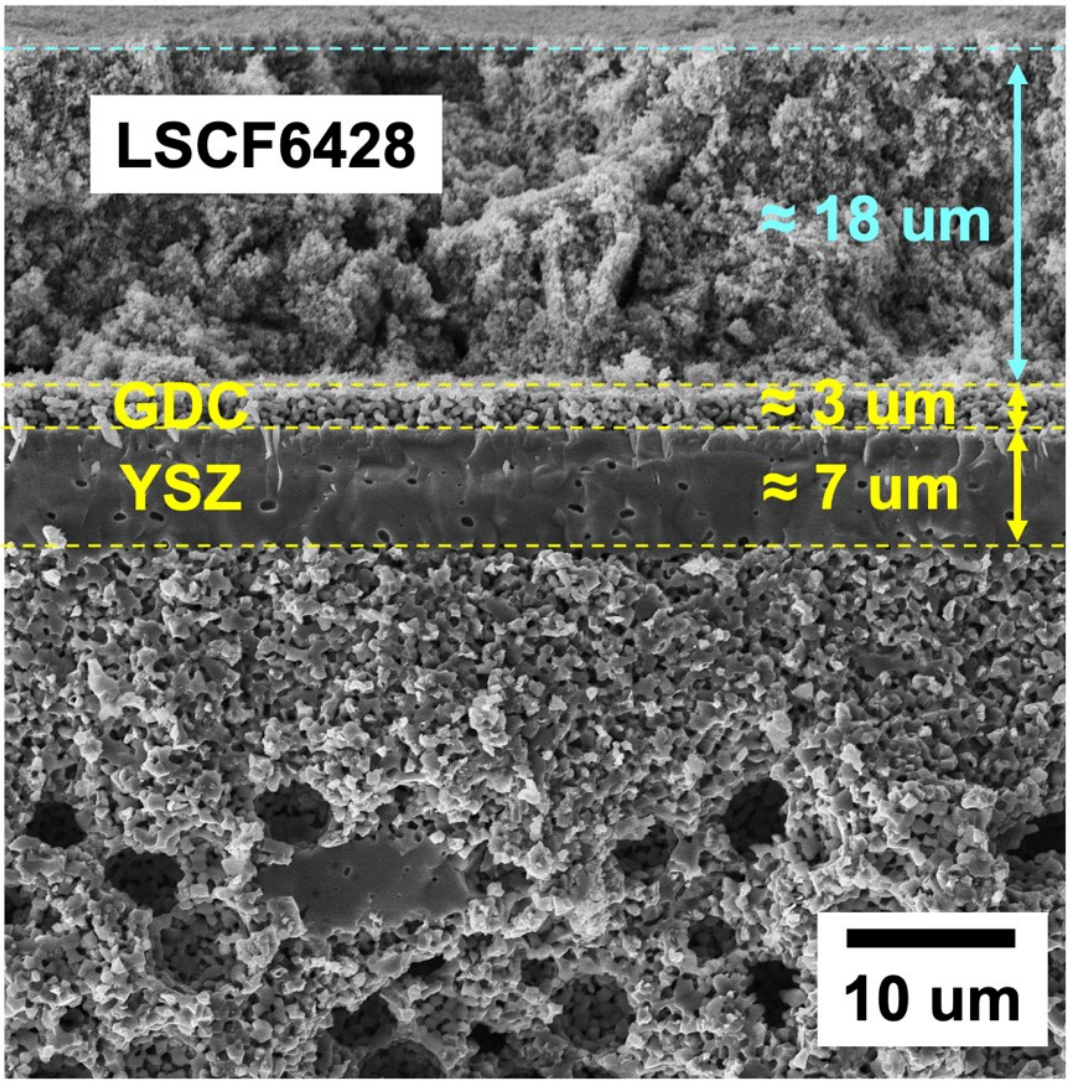

Figure S11. Cross-sectional SEM image of LSCF6428 cell.

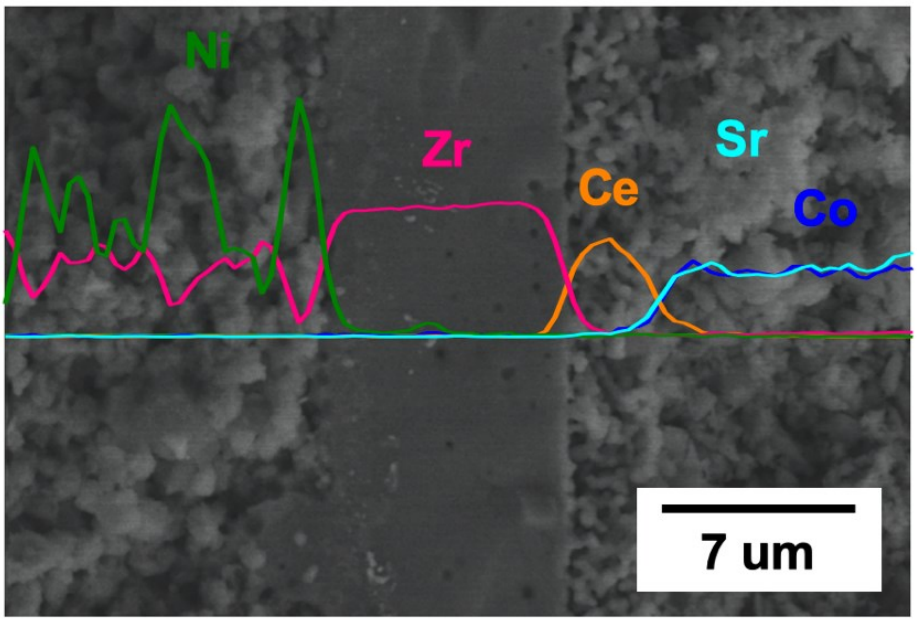

Figure S12. EDX element (Ni, Zr, Ce, Sr, Co) line spectra of a single cell with the LSCF2882 electrode.

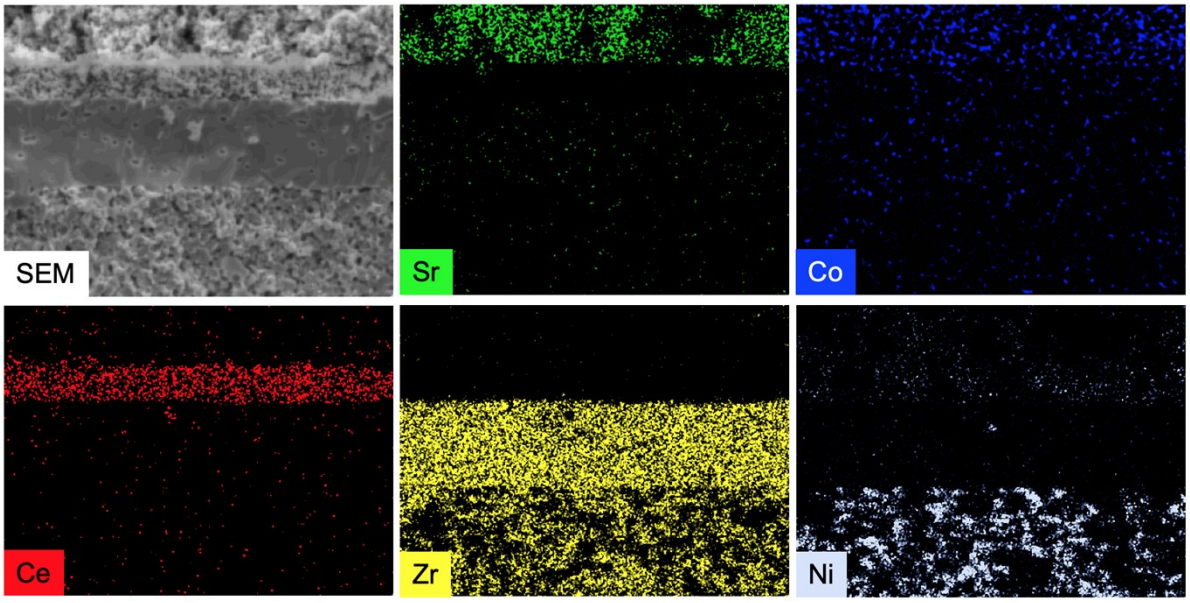

Figure S13. EDX element (Ni, Zr, Ce, Co, Sr) mapping of a single cell with the LSCF2882 electrode after stability test.

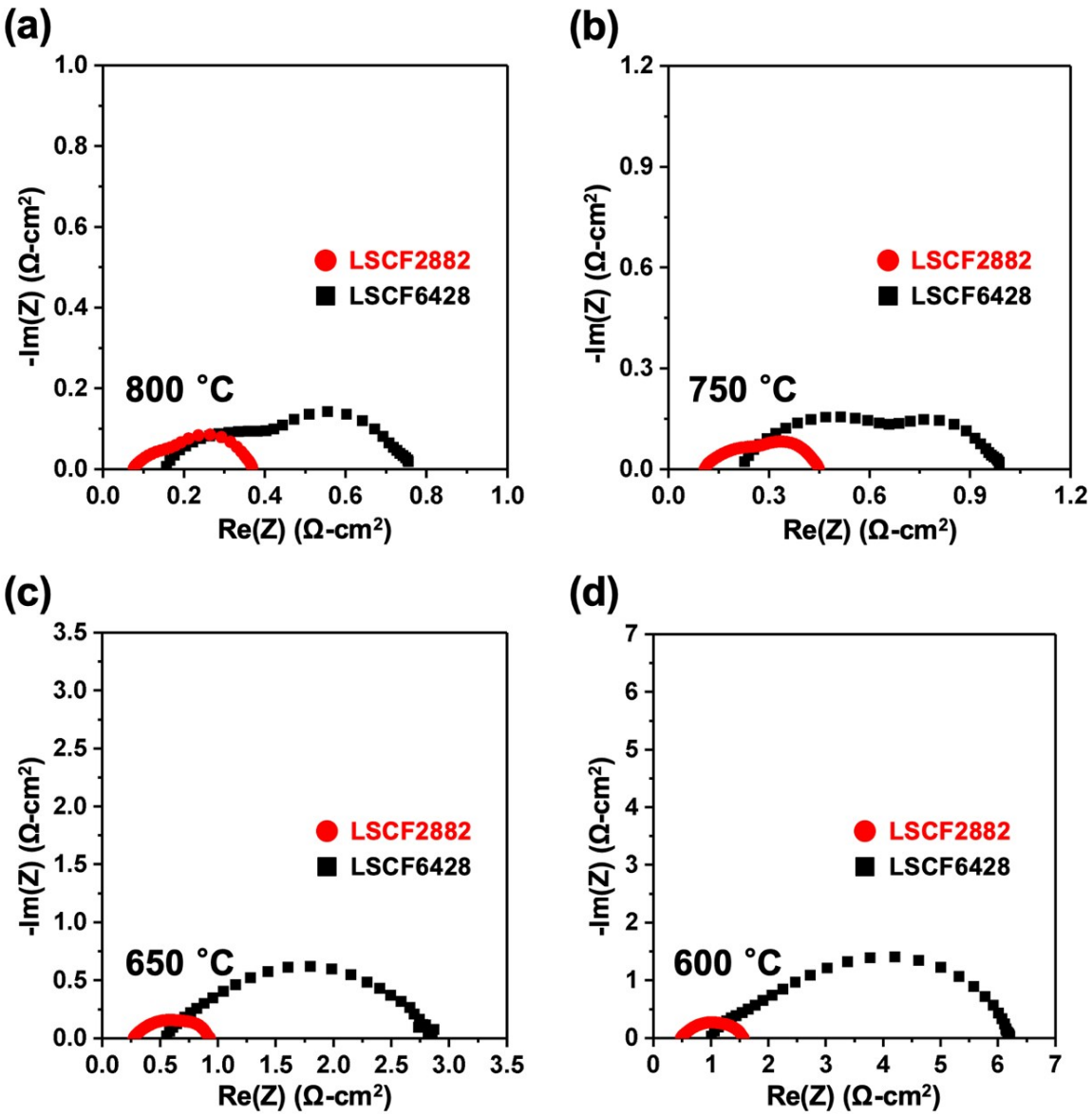

Figure S14. Electrochemical impedance spectra (Nyquist plots) at OCV for LSCF2882 and LSCF6428 cells at different temperatures ranging from 600 to 800 °C.

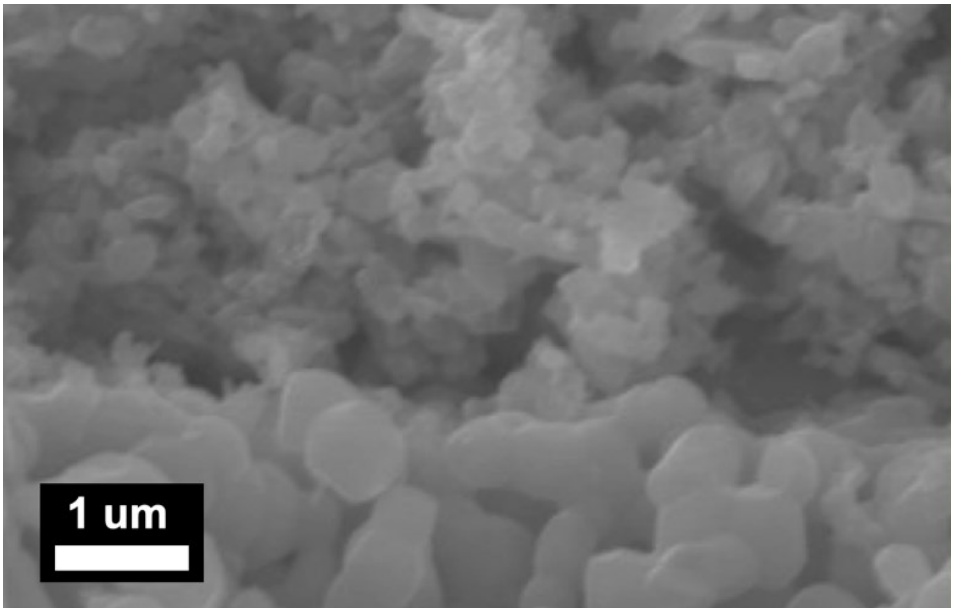

Figure S15. Cross-sectional surface SEM images of the interfaces between the LSCF2882 oxygen electrode and GDC buffer layer after reversible operation conditions.

References

1. Y. Gu, Y. Zhang, Y. Zheng, H. Chen, L. Ge and L. Guo, *Appl. Catal. B Environ*., 2019, 257, 117868.
2. Z. Gao, X. Liu, B. Mergman, Z. Zho, *Journal of Power Sources* 196 (2011) 9195-9203
3. Q. Ni, H. Chen, L. Ge, S. Yu, L. Guo, *Journal of Power Sources* 349 (2017) 130-137
4. F. Lu, T. Xia, Q. Li, J. Wang, L. Huo, H. Zhao, *Appl. Catal. B Environ*., 2019, 249, 19-31.